Following the approach of Reference 5, the authors of Reference 6 introduced a compensating factor η for the increase of the electron effective mass caused by the band structure changes at the Schottky contact into eqn. 4 for recombination velocity, thus proposing eqn. 5. They found η to be equal to 4 by fitting v_{rd} to v_{r0} at equilibrium. Thus factor η is merely a fitting parameter rather than a quantity with real physical sense.

In Fig. 1 different models of recombination velocity are compared. We can see that the model presented here is in good agreement both with the model of Crowell and Sze [3] at low biases (low drift velocity) and with the results of MC simulations at high biases [4]. The discrepancy between the new model (eqn. 2) and the model of Reference 6 is very small, while eqn. 4 significantly overestimates the value of v_r.

Numerical results: To investigate the influence of the varying recombination velocity on the simulation results we used the one-dimensional drift-diffusion simulator with different models of v_r (eqns. 2–5). We followed the numerical procedure described in Reference 5. An Si n-type Schottky diode with 2 μm epilayer doped to 10^{15} cm^{-3} and a barrier height of 0·85 eV was simulated at $T = 300$ K.

In all cases with nonconstant recombination velocity, the current density saturated at $\sim 10^3$ A/cm^2 whereas eqn. 3 with constant v_r predicted a $\sim$15% lower value. At low bias the difference in current densities calculated using the models of eqns. 2 and 4 was greater than 40% which is in contrast with the results of Reference 5. We should point out that the nonlinear dependence of the current density on recombination velocity makes the I-V characteristics insensitive to the value of v_{rd}. Simulated I-V curves corresponding to the models of eqns. 2 and 5 are very close to each other in the whole bias range.

Calculated capacitance-voltage characteristics are shown in Fig. 2. Capacitance was defined as $C = dQ/dV$ where dV is the increment of bias and dQ is the corresponding increment of the charge stored in the semiconductor. At low bias, the diode capacitance is determined by the 'barrier capacitance' and is hardly affected by the value of recombination velocity. However, at high injection level the influence of the boundary condition on the simulated C-V characteristics is substantial and the model of eqn. 3 with constant recombination velocity can overestimate the capacitance significantly.

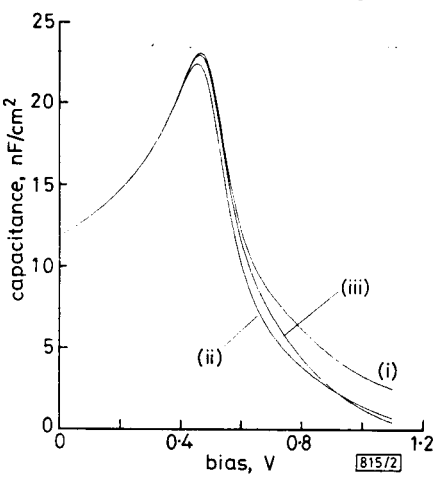

Fig. 2 *Comparison of C-V characteristics calculated with different recombination velocity models*

(i) [3]
(ii) [5]
(iii) this Letter

Conclusions: We propose a new boundary condition for the Schottky barrier diode that is applicable over a wide bias range. The results of the numerical simulation clearly show that the appropriate choice of recombination velocity model is important for accurate simulation of I-V and C-V characteristics.

24th July 1992

A. Shibkov, M. Ershov and V. Ryzhii (*Institute of Physics and Technology of the Russian Academy of Sciences, 25A Krasikov Street, Moscow, 117218, Russia*)

References

1 CHUANG, C. T.: 'On the current-voltage characteristics of epitaxial Schottky barrier diodes', *Solid-State Electron.*, 1984, **27**, pp. 299–304
2 GUO, S. T.: 'A simple model for computer simulation of Schottky-barrier diodes', *Solid-State Electron.*, 1984, **27**, pp. 537–543
3 CROWELL, C. R., and SZE, S. M.: 'Current transport in metal-semiconductor barriers', *Solid-State Electron.*, 1966, **9**, pp. 1035–1047
4 BACCARANI, G., and MAZZONE, A. M.: 'Monte Carlo simulation of current transport in forward-biased Schottky-barrier diodes', *Electron. Lett.*, 1976, **12**, pp. 59–60
5 ADAMS, J., and TANG, T.-W.: 'A revised boundary condition for numerical analysis of Schottky barrier diodes', *IEEE Electron Device Lett.*, 1986, **EDL-7**, pp. 525–527
6 NYLANDER, J. O., MASSZI, F., SELBERHERR, S., and BERG, S.: 'Computer simulation of Schottky contacts with a non-constant recombination velocity', *Solid-State. Electron.*, 1988, **32**, pp. 363–367
7 MAZIAR, C. M., and LUNDSTROM, M. S.: 'Monte Carlo simulation of GaAs Schottky barrier behaviour', *Electron. Lett.*, 1987, **23**, pp. 61–62
8 ADAMS, J. G., and TANG, T.-W.: 'Computer simulation of boundary condition for Schottky barrier diodes', *Electron. Lett.*, 1989, **25**, pp. 1098–1100

644

PICOSECOND SOLITON PULSE COMPRESSOR BASED ON DISPERSION DECREASING FIBRE

S. V. Chernikov, D. J. Richardson, E. M. Dianov and D. N. Payne

Indexing terms: Soliton transmission, Pulse generation, Optical fibres

The Letter reports the adiabatic compression of 2–4 ps pulses from a passively mode-locked all-fibre soliton ring laser operating at 1557 nm down to 230 fs in a 1·6 km dispersion decreasing fibre.

Dispersion decreasing fibres (DDFs) are promising tools for the compression of soliton pulses in the region of 1·4–1·7 μm. It has been shown theoretically [1–3] that picosecond fundamental solitons can be adiabatically compressed during propagation along a fibre with slowly decreasing chromatic dispersion. Providing that the dispersion variation is sufficiently adiabatic, the pulse remains a fundamental soliton as it propagates and conserves the input pulse energy, the soliton duration therefore decreases in proportion to the absolute value of the local dispersion. The behaviour of femtosecond solitons in DDF is more complicated due to the Raman self-scattering and third-order dispersion effects [4]. In addition, a number of soliton lasers have recently been developed including fibre soliton lasers based on erbium-doped fibre amplifiers. Various active and passive mode-locking [5–8] fibre lasers configurations have been demonstrated. Such lasers are capable of generating soliton pulses with duration in both the picosecond and subpicosecond regime. Therefore, optical pulse compressors based on adiabatic soliton compression in DDFs can be conveniently employed to extend the operation range of lasers of this type.

We report the first experimental demonstration of the performance of the picosecond soliton pulse compressor based on DDF. A passive mode-locked erbium fibre ring laser [8] was used as the source of soliton pulses with durations in the range 2–4 ps at wavelengths around 1·55 μm. The experimental configuration is shown in Fig. 1. The laser operation is based on nonlinear polarisation evolution (NLPE) [8]. The polarising isolator ensures unidirectional laser operation and provides for an intensity dependent cavity loss as the intracavity polarisation state changes due to NLPE within the lo-bi fibre section. The lo-bi fibre has a length of 180 m and an effective mode area of 120 μm^2 and a dispersion of $D_1 =$ 17 ps/nm/km at 1·55 μm. The gain is provided by a 3 m section

of erbium-doped fibre with 800 *ppm* Er^{3+} ions, $NA = 0.15$ and $\lambda_{co} = 950$ nm. The 80% output coupler was placed immediately after the amplifier to ensure a high output pulse

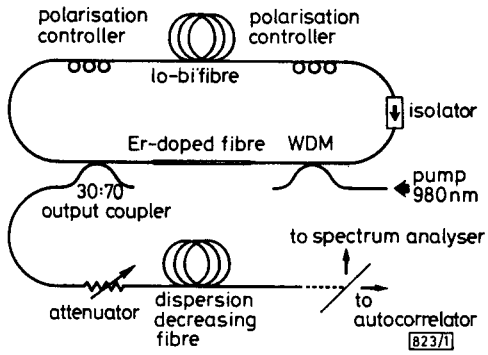

Fig. 1 *Experimental configuration*

energy. The energy of the pulse leaving the laser was four times that of the energy of the fundamental soliton for dispersion D_1, assuming that fundamental soliton pulses circulate within the laser cavity. The system was pumped by a Ti: sapphire laser operating at 978 nm. The launched pump power was actively stabilised by means of a noise-eater circuit based around a Bragg cell placed in front of the launch optics. The CW laser threshold was ~20 mW and mode-locking selfstarted at ~60 mW. By appropriate tuning of the laser polarisation controllers and the input pump power, transform-limited $sech^2$ pulses (time-bandwidth product = 0·32) with durations tunable in the range 2–4 ps could be obtained at the laser output. A typical spectrum and background-free autocorrelation trace measured at the laser output are shown in Fig. 2*a* and *b*, respectively. The results demonstrate a good fit for a 3·5 ps fundamental soliton pulse at 1557 nm with bandwidth 0·73 nm. Note, the small spectral sidelobe characteristic of pulses generated in such fibre based soliton lasers [9]. When the laser polarisation controllers were appropriately tuned these lobes could be suppressed to a level < -30 dB down relative to the peak intensity.

The laser pulses were then coupled into the pulse compressor based on a DDF. The DDF was fabricated by a recently developed technique involving tapering of a singlemode fibre during the pulling process [3]. The fibre had a total length of 1·6 km with a diameter of 160 μm at the input and 115 μm at the output. The dispersion against length profile was designed to have a hyperbolic form. The dispersion as measured at

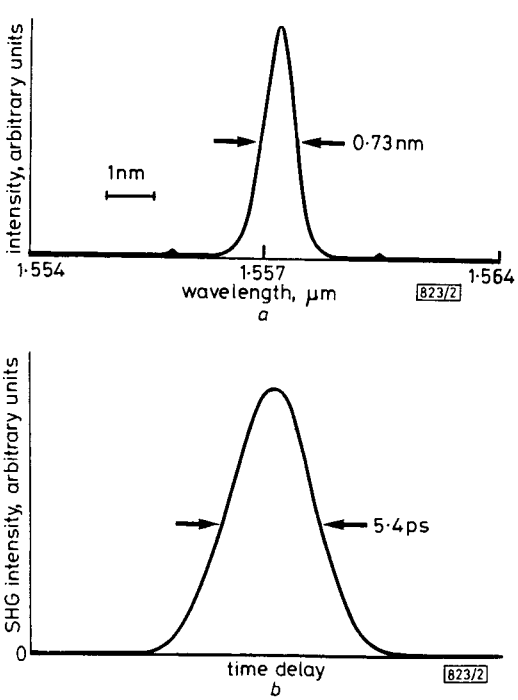

Fig. 2 *Spectrum and autocorrelation trace of 3·5 ps soliton pulses at output of ring laser (DDF input)*

a Spectrum
b Autocorrelation

1550 nm varied between 10 ps/nm/km at the input to 0·5 ps/nm/km at the output. A tunable fibre attenuator was spliced between the laser output and the DDF to enable us to match the pulse energy to that of the fundamental soliton for the dispersion and mode parameters at the DDF input. The spectrum and autocorrelation function at the output of the compressor for the 3·5 ps pulses illustrated in Fig. 2 are shown in Fig. 3*a* and *b*, respectively. It is seen that the pulses have been

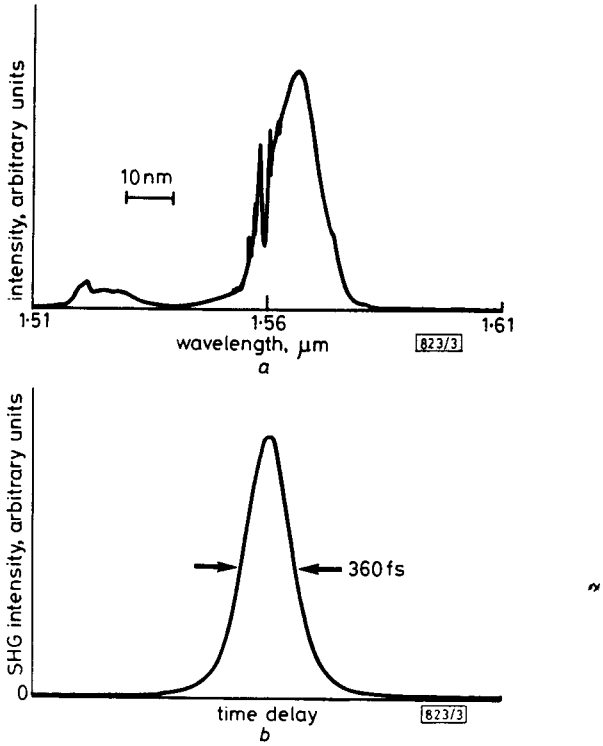

Fig. 3 *Spectrum and autocorrelation trace of 230 fs soliton pulses at output of 1·6 km DDF*

a Spectrum
b Autocorrelation

compressed from 3·5 ps down to 230 fs (representing a compression factor of ~16). The autocorrelation trace of the compressed pulse has a good $sech^2$ form and has no pedestal. The corresponding optical spectrum has broadened from 0·73 to 11 nm. The time-bandwidth product of these pulses is 0·32; the pulses have therefore remained as solitons. The compression process is accompanied by a 10 nm spectral shift due to the Raman self-frequency shift. Note that the appearance of an anti-Stokes component at 1520 nm is associated with soliton propagation in the vicinity of the zero-dispersion wavelength and the effect of third-order dispersion. Such an effect was predicted from the computer simulations of soliton compression in DDFs presented in Reference 4. In addition, it was observed the output soliton duration did not depend significantly on the input soliton pulse width in the pulse tuning range 2–4 ps. This behaviour was expected due to the pulse width stabilisation of femtosecond solitons propagating in DDFs [4]. In more recent experiments the compression of 630 fs solitons from a figure-eight fibre laser down to 100 fs in a 100 m DDF has also been obtained [10].

In conclusion, we have demonstrated a simple fibre pulse compressor based on adiabatic soliton compression in DDF. The advantages of this means of soliton compression lie in its simplicity and the stable, high-quality, polarisation-insensitive compression it provides. In our opinion DDF pulse compressors have great potential for use in conjunction with various mode-locked fibre soliton lasers, ultimately extending their operating range well down into the sub-100 fs regime.

Acknowledgments: This work was in part funded by EEC RACE project R2015 (Artemis).

24th July 1992

D. J. Richardson and D. N. Payne (*Optoelectronics Research Centre, Southampton University, United Kingdom*)

S. V. Chernikov and E. M. Dianov (*General Physics Institute, Moscow, Russia*)

References

1 KAJIMA, K.: 'Compensation of soliton broadening in nonlinear optical fibres with loss', *Opt. Lett.*, 1986, **12**, pp. 54–57

2 KUEHL, H. H.: 'Soliton on an axially nonuniform optical fiber', *J. Opt. Soc. Am. B*, 1988, **5**, pp. 709–715

3 BOGATYREV, V. A., BUBNOV, M. M., DIANOV, E. M., KURKOV, A. S., MAMYSHEV, P. V., PROKHOROV, A. M., SEMENOV, V. A., SEMENOV, S. L., SYSOLIATIN, A. A., CHERNIKOV, S. V., GURIANOV, A. N., DEVYATYKH, G. G., and MIROSHNICHENKO, S. I.: 'Single-mode fiber with chromatic dispersion varying along the length', *J. Lightwave Technol.*, 1991, **LT-9**, pp. 561–566

4 DIANOV, E. M., IVANOV, L. M., MAMYSHEV, P. V., and PRIKHOROV, A. M.: 'High quality, femtosecond fundamental soliton compression in optical fibre with varying dispersion' *in* 'Topical meeting on nonlinear guided wave phenomena: physics and applications', Vol. 2, OSA Tech. Dig. Series, 1989, pp. 157–158

5 SMITH, K., ARMITAGE, J. R., WYATT, R., DORAN, N. J., and KELLY, S. M. J.: 'Erbium fibre soliton laser', *Electron. Lett.*, 1990, **26**, pp. 1149–1151

6 RICHARDSON, D. J., LAMING, R. I., PAYNE, D. N., MATSAS, V., and PHILLIPS, M. W.: 'Self-starting, passively mode-locked fibre laser based on the amplifying Sagnac loop', *Electron. Lett.*, 1991, **27**, pp. 542–544

7 DULING, I. N.: 'Subpicosecond, all-fibre erbium laser', *Electron. Lett.*, 1991, **27**, pp. 544–545

8 MATSAS, V. J., RICHARDSON, D. J., NEWSON, T. P., and PAYNE, D. N.: 'Passively mode-locked, erbium-doped fibre laser based on nonlinear polarisation evolution', *Electron. Lett.*, 1992, **28**, pp. 1391–1393

9 PANDIT, N., NOSKE, D. U., KELLY, S. M. J., and TAYLOR, J. R.: 'Characteristic instabilities of fibre loop soliton lasers', *Electron. Lett.*, 1992, **28**, pp. 455–456

10 CHERNIKOV, S. V., RICHARDSON, D. J., DIANOV, E. M., and PAYNE, D. N.: 'Compression of pulses from soliton fibre lasers in dispersion decreasing fibre', Tech. Dig. Eighth Conf. on Ultrafast Phenomena, (Antibes), Postdeadline paper FC31, 1992

LOW THRESHOLD FS-BH LASER ON *p*-InP SUBSTRATE GROWN BY ALL-MOCVD

Y. Ohkura, T. Kimura, T. Nishimura, K. Mizuguchi and T. Murotani

Indexing terms: Lasers, Semiconductor lasers, Chemical vapour deposition

A novel FS-BH laser structure using the selective growth characteristics of MOCVD on crystal facets has been developed. A threshold current as low as 12 mA and output power of 40 mW under CW operation have been achieved in the laser.

Introduction: There is strong demand for long wavelength laser arrays for computer links and telecommunication systems. In such laser arrays, *p*-InP substrate is preferable to *n*-InP substrate from the viewpoint of high speed operation, because high speed *npn* bipolar transistors are available.

Currently, *p*-InP substrate lasers are produced by LPE or MOCVD–LPE hybrid processes [1]. In such processes, however, the uniformity and reproducibility of the layer thickness are not sufficient for fabrication of the laser arrays.

It is well known that MOCVD enables excellent controllability and uniformity of the growth thickness. Many papers have been published on all-MOCVD grown on *n*-InP substrates [2]. However, there are few reports, to the best of our knowledge, on all-MOCVD grown lasers on *p*-InP substrates, mainly due to the difficulties experienced in correctly placing the current blocking structure with respect to the active region.

We report, for the first time, the results of lasers grown on the *p*-InP substrate by all-MOCVD.

Leakage current of p-InP substrate lasers: For buried-heterostructure lasers on *p*-InP substrates, it is necessary to minimise the leakage current flowing outside the active region by forming the *n*-InP current blocking layer very close to the active layer but with no contact to the *n*-InP cladding layer. Large leakage current flows through the *n*-InP current blocking layer when the *n*-InP current blocking layer is linked to the *n*-InP cladding layer, because the resistivity of the *n*-InP current blocking layer is small. When the *n*-InP current blocking layer does not make contact with the *n*-InP cladding layer, leakage current flows through the *p*-InP filling layer (see Fig. 1). In this case, the amount of leakage current is determined by the space between the *n*-InP blocking layer and the active layer (which we define as the space leakage path width).

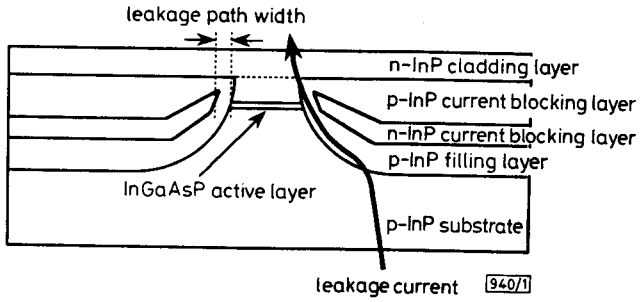

Fig. 1 *Leakage current path of BH lasers on p substrate*

Buried-growth characteristic: To realise the current confinement structure on *p*-InP substrate by MOCVD, we have investigted the growth characteristics on a nonre-entrant mesa [3] stripe with SiO_2 mask on the DH wafer. The mesa stripe orientation is in the ⟨110⟩ direction. Fig. 2 schematically shows the growth profile. In the first stage of buried growth, the (111)B and (221)B facets where the growth rate is found to be zero and very slow, respectively, are formed on the mesa side wall. The next stage, in which we grow the *n*-InP current

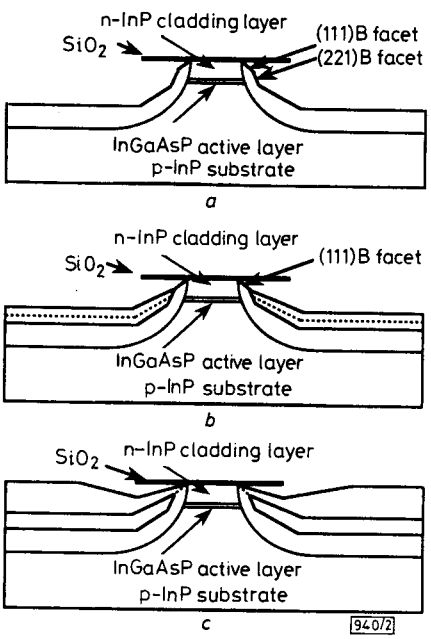

Fig. 2 *MOCVD growth profile on the nonre-entrant mesa stripe*
a–c: stages 1–3, respectively

blocking layer without it making contact with the *n*-InP cladding layer, involves forming (111)B and (221)B facets, until the (221)B disappears. The layer grown in this stage does not make contact with the *n*-cladding layer because the non-growth (111)B facet is already formed and the distance between this layer and the active layer does not depend on the thickness of the layer grown in the first stage for formation of the (221)B facet. The growth on the (111)B facet then starts and the mesa is embedded in the third stage.

Thus the *n*-InP current blocking layer can be formed close to the active layer, without it making contact with the *n*-InP cladding layer, by forming the *p*-InP filling layer, the *n*-InP current blocking layer and the *p*-InP blocking layer in the first, second and third stages, respectively.

We have also investigated the growth characteristics on a vertical mesa stripe and confirmed that the *n*-InP current blocking layer can be formed without it making contact with the *n*-InP cladding layer. In this case, the (111)B facet is formed on the top of the mesa side wall, but the (221)B facet is